Periodic Gaussian Expansions of Hydrogenic Orbitals: A Spatial and Frequency Domain Analysis

EL HOUSSAIN AIT MANSOUR[1], ABDELAAZIZ OUAHROUCH[2]

[1]KEAS Group
Department of Engineering, 23 Rue Paul Hroult, 38190 Villard-Bonnoty,
FRANCE

[2]Ibn Zohr University, Biotechnology, Materials and Environment Laboratory, Riad Salam, Agadir
80000
MOROCCO

Abstract: In this paper, we investigate the properties and applications of the Periodic Gaussian basis function for Hydrogenatom wavefunctions. We derive analytical expressions for the expansions of 1s, 2s, 2p, 3s, 3p and 3d-type orbitals in one, two and three dimensions, and compare their accuracy and efficiency with the conventional Slater-type orbitals. We show that the Periodic Gaussian function can represent periodic Hydrogenic orbitals in Cartesian 3D space with fewer basis functions, and that its Fourier transform reveals interesting insights into the physical characteristics of Hydrogen-atom wavefunctions, such as the quantization of energy levels. Our results demonstrate the potential of the Periodic Gaussian basis function for computational chemistry applications involving periodic systems.

Key–Words: Periodic Gaussian basis function, Hydrogen-atom wavefunctions, spatial and frequency domains, Slater-type orbitals, Chemistry computation, Fourier transform, Quantization phenomenon.

Received: May 5, 2024. Revised: August 4, 2024. Accepted: September 7, 2024. Published: October 23, 2024.

1 Introduction

Slater-type basis functions are widely used to calculate atomic and molecular orbitals. The analytical expansion of Slater-type basis functions has successfully achieved Hartree-Fock solutions and *ab initio* methods for single atoms and diatomic molecules [3, 4]. However, the computation of integrals for multicenter molecules, many-body systems and large-scale atoms faces significant challenges. On the other hand, Gaussian-type orbitals were originally developed by John C. Slater [1] to describe electronic wavefunctions, because they simplify the integration over Gaussian functions compared to Slater-type orbitals. Recent work with large Gaussian basis sets has shown the efficiency of Hartree-Fock (HF) wavefunction calculations for molecular integrals [2]. However, the Gaussian basis functions do not behave correctly near the nucleus, and decay faster than Slater basis functions far from the nucleus [5, 6, 7]. The conventional definition of the normalized radial part of Slater-type orbitals [8, 9] is given by

$$R_{_S}(r,\zeta) = N_{_S}(\zeta) r^{n-1} \exp(-\zeta|r|) \tag{1}$$

where ζ is the exponent parameter for Slater-type orbitals. We use α as the exponent parameter for Gaussian-type orbitals. The normalized radial part of Gaussian-type orbitals [10, 11] can be written as:

$$R_{_G}(r,\alpha) = N_{_G}(\alpha) r^{n-1} \exp(-\alpha r^2) \tag{2}$$

To rephrase in English: "Moreover, it seems that none of the existing types of orbitals can provide a clear and definitive interpretation for molecular calculations. Slater-type Orbitals (STO's) are good at capturing the specific behavior of an electron near a nucleus. Gaussian-Type Orbitals (GTO's) are convenient for computing molecular integrals. However, both STO's and GTO's have a major drawback: they assume that the electron wavefunctions are only dependent on one nucleus. This is a mathematical property of the Gaussian and Exponential decay basis functions, which have single centers and decay quickly away from the nucleus. This is a significant limitation, as real macroscopic atomic structures [12, 13, 14] consist of multiple centers, many-body interactions and emergent phenomena. Therefore, STO's and GTO's are not very effective at connecting single orbitals with macroscopic atomic structure behaviors, such as the quantization effects observed in quantum mechanics.

We can write STO's orbitals as a sum of Gaussian basis functions with M terms, where c_i are the expansion coefficients and α_i are the exponent parameters. The formula for the linear combination of GTO's that approximates STO's is given by [9].

$$R_{_S}(r,\zeta) \approx R_{_G}(r,\alpha_i) \approx r^{n-1} \sum_{i=1}^{M} c_i \exp(-\alpha_i r^2) \tag{3}$$

This research aims to develop a novel Periodic Gaussian basis function for Hydrogen-atom wavefunctions that includes 3d-type orbital and to analyze its physical and mathematical properties in

relation to quantization phenomenon. In this paper, we use a single Gaussian (M=1) in Eq. 3 basis function $\exp(-\alpha r^2)$ to expand both Slater-type basis function $\exp(-\zeta|r|)$ and Periodic Gaussian basis function $\psi(r)$ as shown in Figure. 1. We detail the spatial and frequency analysis in sections II.1 and II.2. We describe the canonical Hydrogenic wavefunctions in section II.3. We discuss the analytical and simulation results in Section. III.

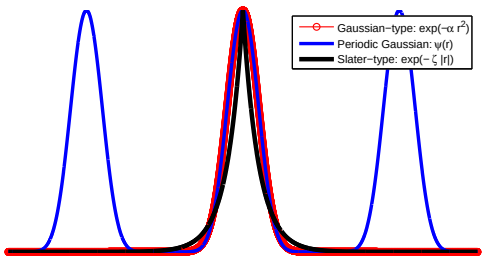

Figure 1: Normalized Slater-type, Gaussian-type and Periodic Gaussian $\psi(r)$ basis functions for given distance to nucleus (r).

2 Periodic Gaussian basis Function

2.1 Spatial Analysis

The Gaussian basis function $g_1(r)$ has two parameters: (μ) and (σ). The former is the center of the Gaussian, while the latter is the standard deviation that measures how far the values are spread from the center. α is the Gaussian exponent parameter that is the inverse of the variance (σ^2).

$$g_1(\sigma,\mu)(r) = \frac{1}{\sigma\sqrt{2\pi}}\exp\left(-\frac{1}{2\sigma^2}\left(r-\mu\right)^2\right) = A\exp\left(-\alpha r_\mu^2\right),$$
$$where\ A = \frac{1}{\sigma\sqrt{2\pi}},\ \alpha = \frac{1}{2\sigma^2},\ r_\mu = r-\mu \tag{4}$$

Let f_0 be the natural spatial frequency or wave-number that describes the periodic atomic structure in space, measured in cycles per meter m^{-1}, which is the inverse of the wavelength $\lambda = 1/f_0$ in meter. We use $\omega_0 = 2\pi f_0 = 2\pi/\lambda$ to denote the atomic angular wave-number in rad/m. The Gaussian order is determined by the parameter n [15]. Then, the radial Periodic Gaussian basis function $\psi_1(r)$ can be written as

$$\psi_1(n,f_0)(r) = A\sin^n\left(2\pi f_0 r\right) = A\sin^n\left(\omega_0 r\right),\ n\geq 1 \tag{5}$$

The common units for measuring the size of atoms and the distance from the nucleus are nanometer (1 nm = 10^{-9} m) and Angstrom (1 $\mathring{A}$ = 10^{-10} m). The units of (r) and (λ) should be consistent. Then, the ratio $\frac{r}{\lambda}$ is independent of the unit of distance as follows

$$\psi_1(r) = A\sin^n\left(2\pi\frac{r}{\lambda}\right) = A\sin^n\left(2\pi\frac{r\cdot 10^{-9}}{\lambda\cdot 10^{-9}}\right) \tag{6}$$

Given (σ,μ), let β be the ratio of σ to μ and N be the number of spatial periods. Then, the computation of the radial periodic Gaussian basis function with (n, f_0) parameters is simplified to the expression in Eq. (7). This equation shows the analytical transformation from the true Gaussian $g_1(\sigma,\mu)(r)$ to the approximate Gaussian $\psi_1(n,f_0)(r)$ basis functions with an error less than 10^{-6} [15].

$$g_1(r) \approx \quad \psi_1(r) = A\sin^n\left(\omega_0 r\right) = A\sin^n\left(\frac{\pi r}{2\mu}\right)$$
$$where\begin{cases} \sigma(n) & = \mu\left(1-\frac{2}{\pi}\arcsin\left(\exp\left(-\frac{1}{2n}\right)\right)\right), \\ n(\sigma) & = -\frac{1}{2\ln\left(\sin\left(\frac{\pi}{2}(1-\beta)\right)\right)}, \\ \beta & = \frac{\sigma}{\mu},\ 0<\beta<1,\ \mu=\frac{\lambda}{4}=\frac{1}{4f_0},\ 0\leq r\leq 2\mu N \end{cases} \tag{7}$$

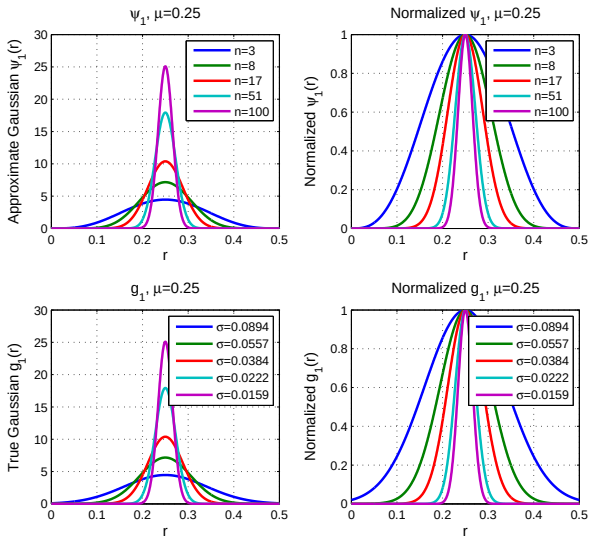

Figure 2: True Gaussian basis function $g_1(r)$ and its approximation $\psi_1(r)$ versus n, $\mu = \frac{\lambda}{4} = 1/4$, N=1: $0 \leq r \leq \frac{\lambda}{2}$.

Figures 2 and 3 describe a single (N=1) periodic Gaussian $\psi_1(r)$ relative to a single true Gaussian, $g_1(r)$ and round a Gaussian number (N=3) versus the n parameter as shown in Eq. (7). The periodic Gaussian expansion decays rapidly as n increases as an inverse effect of the σ parameter. As mentioned in [15] and shown in Fig. 2, the periodic Gaussian approximation model gave the best accuracy compared to the original Gaussian function with Odd and even values of n imply that the periodic Gaussian cells are symmetric and antisymmetric , as shown in Fig. 3. From this figure,

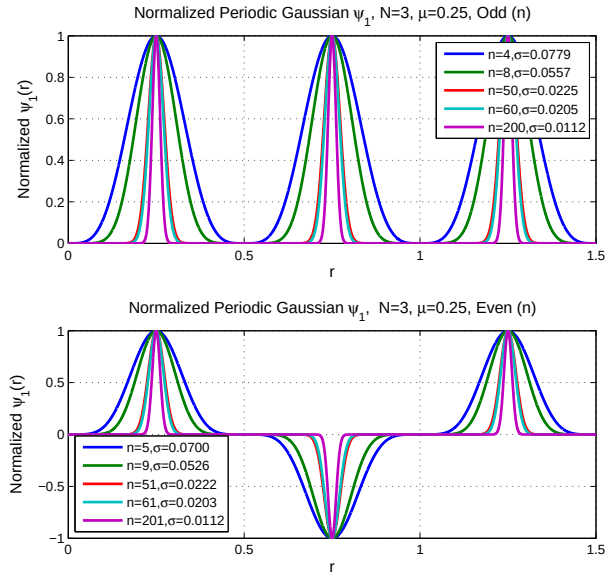

Figure 3: Normalized periodic Gaussian $\psi_1(r)$ versus n for $\mu = \frac{\lambda}{4} = 1/4$, N=3: $0 \leq r \leq 3\frac{\lambda}{2}$

the highest (n) value seems produced similar (σ) as $(n+1)$ (n=200 $\Rightarrow\sigma\approx$ 0.0112, n=201$\Rightarrow\sigma\approx$ 0.0112). In the following, we extend the periodic Gaussian basis function to 2D and 3D dimensions in Cartesian coordinates using illustrative examples.

(m) denotes the dimension number. For periodically high Gaussian parameters, a combination of multiple methods is used in a one-dimensional Gaussian method. Considering r=$\{r_1, r_2, ..., r_m\}$ point coordinates in m-dimensional space, we have

$$\begin{aligned} g_m(r) &= g_1(r_1)\cdot g_1(r_2)\cdot ...\cdot g_1(r_m) = \prod_{i=1}^{m} g_1(r_i) \\ &= A^m \exp\left(-\alpha\left(r_1^2 + r_2^2 + ... + r_m^2\right)\right) \\ &= A^m \exp\left(-\alpha r^2\right),\ r = \sqrt{r_1^2 + r_2^2 + ... + r_m^2} \end{aligned} \tag{8}$$

If the terms (5) and (7) are replaced by (9), then the m-dimensional periodic Gaussians $\psi_m(r)$ and $\psi_3(r)$ can be expressed by

$$\begin{aligned} \psi_m(r) &= \psi_m(r_1, r_2, ..., r_m) = A^m \prod_{i=1}^{m} \psi_1(r_i) \\ &= A^m \prod_{i=1}^{m} \sin^n\left(\omega_0 r_i\right) \\ \psi_3(r) &= A^3\left(\sin(\omega_0 r_1)\cdot\sin(\omega_0 r_2)\sin(\omega_0 r_3)\right)^n, \\ where\ r &= \sqrt{r_1^2 + r_2^2 + r_3^2},\ A^3 = \left(\frac{1}{2\pi\sigma^2}\right)^{\frac{3}{2}} = \left(\frac{\alpha}{\pi}\right)^{\frac{3}{2}} \end{aligned} \tag{9}$$

Periodic Gaussian basis functions in 1D, 2D, and 3D space are described in Fig. 4, together with $\{r_1, r_2, r_3\} \in \{0,\ N\frac{\lambda}{2}\}$, λ=1. The $\psi_3(r)$ function has a spherical isosurface shape, as can be seen in the image. The only factors influencing the number of Gaussian cells N_b are the dimensions parameters (m,N) and periods. One cell, four cells for $\psi_2(r)$(N=3,m=2), eight cells for $\psi_3(r)$(N=3,m=3), and $N_b = N^m$ for $\psi_m(r), N > 1$ make up the $\psi_1(r)$ (N=3,m=1). The number of spherical objects per volume unit in 3D space, or number density, is indicated by the N_b parameter. It can be applied to 3D space to determine the size architecture of periodic spherical objects such as molecules and atoms.

The periodic Gaussian basis function's n parameter's interest is seen in Fig. 5. The n parameter determines the periodic Gaussian size. While the distance from the nucleus remained constant, the size of the cell decreased as n increased. It is commonly known that the Gaussian center μ is centered in $\pm 3\sigma$ approximately 99% of the Gaussian energy. Moreover, the inverse effect of the standard deviation σ on n is given by equation (7). A rise in n caused a void to appear between every two cell neighbors. This parameter is interesting for adjusting the size and spacing of spherical objects within a certain volume. We shall examine the periodic Gaussian basis function analytically in the spatial frequency domain in the sections that follow.

2.2 Frequency Analysis

Here we compute Fourier Transforms (FT) between an infinite sum of shifted single Gaussian functions and a periodic Gaussian basis function. The only function we'll utilize is 1D. This produces outcomes that are both intriguing and straightforward to understand in the analysis. With ν representing the wave number in the spatial frequency in m^{-1}, let $G_1(\nu)$ represent the FT of $g_1(r)$. As a result, $G_1(\nu)$ can be expressed as

$$\begin{aligned} G_1(\nu) &= FT\left[g_1(r)\right] = \underbrace{A_1 \exp\left(-\alpha_1\nu^2\right)}_{continuous\ Gaussian}, \\ with\ A_1 &= A\sqrt{\pi/\alpha},\ \alpha_1 = \pi^2/\alpha \end{aligned} \tag{10}$$

Let α_1 be the Gaussian exponential parameter in the frequency domain, and N_1 be the number of shifted Gaussian cells by μ. Let

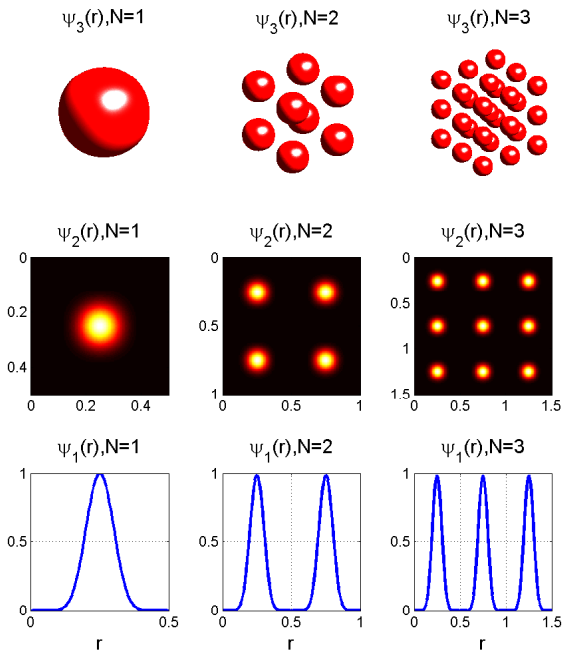

Figure 4: From top to bottom $\psi_3(r)$, $\psi_2(r)$ and $\psi_1(r)$ for N={1,2,3}, n=10, f_0=1, $0 \leq r_1, r_2, r_3 \leq 1.5$, 128×128×128 mesh elements.

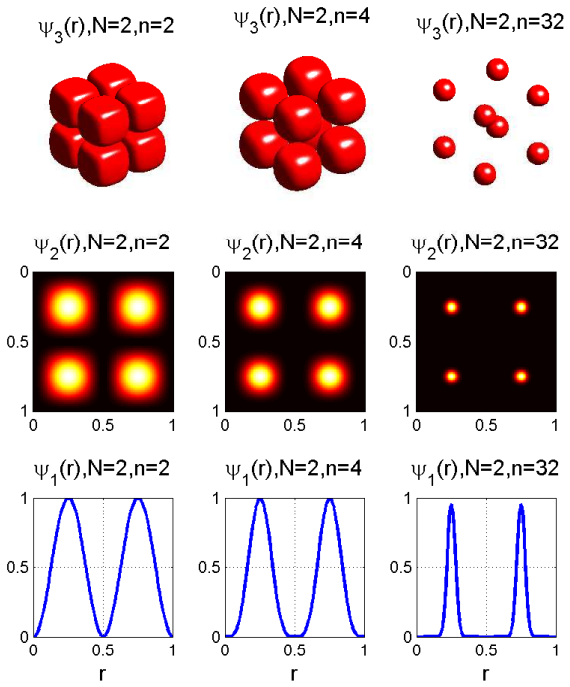

Figure 5: From top to bottom $\psi_3(r)$, $\psi_2(r)$ and $\psi_1(r)$ for for n={2,4,32}, N=2, f_0=1, $0 \leq r_1, r_2, r_3 \leq 1$, 128×128×128 mesh elements.

$g(r)$ represent the infinite sum of $g_1(r)$ shifted Gaussian cells. Using the property of convolutional product ($\oplus$), we get

$$g(r) = \sum_{N_1=-\infty}^{\infty} g_1(r - N_1\mu) = g_1(r) \oplus \sum_{-\infty}^{\infty} \delta(r - N_1\mu) \tag{11}$$

let δ denotes Dirac delta distribution and $G(\nu)$ the FT of $g(r)$. Then, we obtain

$$\begin{aligned} G(\nu) &= FT\Big[g_1(r)\Big] \\ &= \sum_{-\infty}^{\infty} FT\Big[g_1(r)\Big] \cdot FT\Big[\delta(r - N_1\mu)\Big] \\ &= \frac{1}{\mu}\sum_{-\infty}^{\infty} G_1(\nu) \cdot \delta\Big(\nu - \frac{N_1}{\mu}\Big) \\ &= \sum_{-\infty}^{\infty} \frac{1}{\mu} \underbrace{G_1\Big(\nu - \frac{N_1}{\mu}\Big)}_{discrete\ Gaussian} \delta\Big(\nu - \frac{N_1}{\mu}\Big) \end{aligned} \tag{12}$$

Let us now compute $\psi_1(r)$, a Periodic Gaussian basis function. To start, in order to reduce mathematical complexity, we provide an Euler linearization of the power-sine function. Let ω_i represent angular pulsation for specified harmonics (i), (j) be an imaginary number with j^2=-1, and $\binom{n}{i}$ denote binomial coefficients. Next up, we have

$$\begin{aligned} \psi_1(r)/A &= \sin^n\Big(\omega_0 r\Big) \\ &= \frac{1}{(2j)^n}\sum_{i=0}^{n}\binom{n}{i}\Big(-1\Big)^{n-i} \cdot \exp\Big(j\omega_i r\Big) \\ where\ \binom{n}{i} &= \frac{n!}{i!(n-i)!},\ \omega_i = \omega_0(2i-n),\ n > 0 \in \mathbb{N}, \end{aligned} \tag{13}$$

Then the FT $\Psi_1(\nu)$ of $\psi_1(r)$ described in Eq. (13) using shifting property in frequency domain is expressed by

$$\begin{aligned} \Psi_1(\nu)/A &= FT\Big[\psi_1(r)/A\Big] = FT\Big[\sin^n\Big(\omega_0 r\Big)\Big] \\ &= \frac{1}{(2j)^n}\sum_{i=0}^{n}\binom{n}{i}\Big(-1\Big)^{n-i} \cdot \delta\Big(\nu - f_i\Big) \\ where\ \omega_i &= 2\pi f_0(2i-n) = 2\pi f_i,\ f_i = f_0(2i-n) \end{aligned} \tag{14}$$

Additionally, $\mu = \frac{\lambda}{4}$ can be used to describe $\psi_1(r)$ with the cosine function via left translation. This results in a spatial domain that is centered Gaussian. Since $\Psi_1^c(\nu)$ is the $\psi_1(r)$ FT, we get

$$\psi_1(r+\mu)/A = \cos^n\left(\omega_0 r\right) = \frac{1}{2^n}\sum_{i=0}^{n}\binom{n}{i}\exp\left(j\omega_i r\right)$$
$$\Psi_1^c(\nu)/A = FT\Big[\psi_1(r+\mu)/A\Big] = \frac{1}{2^n}\sum_{i=0}^{n}\binom{n}{i}\delta\Big(\nu - f_i\Big) \tag{15}$$

For both the (14) and (15) equations, the FT modulus is given by, and it stays constant finely.

$$||\Psi_1(\nu)|| = ||\Psi_1^c(\nu)|| = \sum_{i=0}^{n}\underbrace{\frac{A}{2^n}\binom{n}{i}}_{discrete\ coefficients}\delta\Big(\nu - f_i\Big) \tag{16}$$

2.3 Hydrogenic Wave-functions

In this section, we present the Cartesian expansions of STO orbitals. We apply a first approximation to simplify the mathematical expression, using GTO and Periodic Gaussian (PG) basis functions (STO $\approx$ STO-1G $\approx$ STO-1PG) as shown in Eq. (17). Moreover, we provide analytical formulas for primary STO orbitals including 3d-type and their corresponding canonical periodic Gaussian orbitals.

$$\underbrace{A\cdot\exp\Big(-\zeta r\Big)}_{STO} \approx \overbrace{B\cdot\exp\Big(-\alpha r^2\Big)}^{STO-1G} \approx \underbrace{C\cdot\psi_3(r)}_{STO-1PG} \tag{17}$$
$$A, B, C : Normalization\ constants$$

Let us now define the meaning of the exponent parameter (ζ) in Slater-type orbitals. We use the following constants and parameters: m_e: electron mass, q_e: elementary charge, Z: number of protons, h: Planck's constant, ϵ_0: vacuum permittivity and a_0 is the Bohr radius. The ζ parameter is linearly proportional to the number of protons Z and the electron mass m_e as shown in Eq. (18). A higher ζ means a larger and heavier particle.

$$\zeta = \frac{Z}{a_0} = Zm_e\underbrace{\frac{\pi q_e^2}{h^2\epsilon_0}}_{\zeta_0} = Zm_e\zeta_0,\ where\ a_0 = \frac{h^2\epsilon_0}{m_e\pi q_e^2} \tag{18}$$

We can now compute the canonical forms of the Periodic Hydrogenic orbitals, by considering each wavefunction individually. Let $\psi_{1s}(r)$, $\psi_{2s}(r)$, $\psi_{2px}(r)$, $\psi_{2py}(r)$ and $\psi_{2pz}(r)$ represent the first five wavefunctions of the $(1s)$, $(2s)$, $(2px)$, $(2py)$ and $(2pz)$ orbitals, respectively. The canonical forms of the other wavefunctions, including the 3d-type ones, are given in the Appendix section. Then, we obtain

$$\begin{aligned}
\psi_{1s}(r) &= A_{1s}\exp\Big(-\zeta r\Big),\ A_{1s} = \sqrt{\frac{\zeta^3}{\pi}}\\
&\approx B_{1s}\exp\Big(-\alpha r^2\Big),\ N=1\\
&\approx \underbrace{\frac{B_{1s}}{A^3}}_{constant\ B'_{1s}}\quad \psi_3(r) = B'_{1s}\psi_3(r),\ N\geq 1
\end{aligned} \tag{19}$$

$$\begin{aligned}
\psi_{2s}(r) &= A_{2s}\Big(2-\zeta r\Big)\exp\Big(-\frac{\zeta}{2}r\Big),\ A_{2s} = \sqrt{\frac{\zeta^3}{32\pi}}\\
&= A_{2s}\Big(2-\zeta r\Big)\exp\Big(-\frac{\zeta}{2}r\Big)\\
let\ \psi_{1s}^{\frac{1}{2}} &= \Big[A_{1s}\exp\Big(-\zeta r\Big)\Big]^{\frac{1}{2}} = \sqrt{A_{1s}}\exp\Big(-\frac{\zeta}{2}r\Big)\\
&\Rightarrow \exp\Big(-\frac{\zeta}{2}r\Big) = \Big(\frac{\psi_{1s}}{A_{1s}}\Big)^{\frac{1}{2}}\\
then\ \psi_{2s}(r) &= A_{2s}\Big(2-\zeta r\Big)\Big(\frac{\psi_{1s}}{A_{1s}}\Big)^{\frac{1}{2}}\\
&= \underbrace{\frac{A_{2s}}{\sqrt{A_{1s}}}}_{A'_{2s}}\Big(2-\zeta r\Big)\psi_{1s}^{\frac{1}{2}}\\
&\approx A'_{2s}\Big(2-\zeta r\Big)\Big(\underbrace{B_{1s}\exp\Big(-\alpha r^2\Big)}_{\approx\psi_{1s}(r)}\Big)^{\frac{1}{2}}\\
let\ \Big(\psi_{1s}^{\frac{1}{2}}\Big)^{(1)} &= \frac{\partial}{\partial r}\Big(\psi_{1s}^{\frac{1}{2}}\Big) = -\alpha r\psi_{1s}^{\frac{1}{2}}\\
&\Rightarrow r\psi_{1s}^{\frac{1}{2}} = -\frac{1}{\alpha}\Big(\psi_{1s}^{\frac{1}{2}}\Big)^{(1)}\\
then\ \psi_{2s}(r) &\approx A'_{2s}\Big(2\psi_{1s}^{\frac{1}{2}} + \frac{\zeta}{\alpha}\Big(\psi_{1s}^{\frac{1}{2}}\Big)^{(1)}\Big)
\end{aligned} \tag{20}$$

$$\begin{aligned}
\psi_{2pz}(r) &= A_{2pz}\zeta z\exp\Big(-\frac{\zeta}{2}r\Big),\ A_{2pz} = A_{2s}\\
&= \frac{\zeta A_{2pz}}{\sqrt{A_{1s}}}z\psi_{1s}^{\frac{1}{2}} = A'_{2pz}\zeta z\psi_{1s}^{\frac{1}{2}}\\
let\ \Big(\psi_{1s}^{\frac{1}{2}}\Big)^{(1z)} &= \frac{\partial}{\partial z}\Big(\psi_{1s}^{\frac{1}{2}}\Big) \approx -\alpha z\psi_{1s}^{\frac{1}{2}}\\
&\Rightarrow z\psi_{1s}^{\frac{1}{2}} \approx -\frac{1}{\alpha}\Big(\psi_{1s}^{\frac{1}{2}}\Big)^{(1z)}\\
then:\ \psi_{2pz}(r) &\approx -A'_{2pz}\frac{\zeta}{\alpha}\Big(\psi_{1s}^{\frac{1}{2}}\Big)^{(1z)}\\
\psi_{2py}(r) &\approx -A'_{2py}\frac{\zeta}{\alpha}\Big(\psi_{1s}^{\frac{1}{2}}\Big)^{(1y)}\\
\psi_{2pr}(r) &\approx -A'_{2px}\frac{\zeta}{\alpha}\Big(\psi_{1s}^{\frac{1}{2}}\Big)^{(1x)}
\end{aligned} \tag{21}$$

$$
\begin{aligned}
with \left(\psi_{1s}^{\frac{1}{2}}\right)^{(1x)} &= \left(A_{1s}^{\frac{1}{2}}\left(\sin(\omega_0 x)\sin(\omega_0 y)\sin(\omega_0 z)\right)^{\frac{n}{2}}\right)^{(1x)} \\
&= A_{1s}^{\frac{1}{2}}\frac{n}{2}\omega_0\cos(\omega_0 x)\sin^{\frac{n}{2}-1}(\omega_0 x)\cdot \\
&\quad \left(\sin(\omega_0 y)\sin(\omega_0 z)\right)^{\frac{n}{2}} \\
\frac{n}{2} >> 1 \Rightarrow \left(\psi_{1s}^{\frac{1}{2}}\right)^{(1x)} &\approx \frac{n\omega_0}{2}\cos(\omega_0 x)\psi_{1s}^{\frac{1}{2}} \\
\Rightarrow \left(\psi_{1s}^{\frac{1}{2}}\right)^{(1y)} &\approx \frac{n\omega_0}{2}\cos(\omega_0 y)\psi_{1s}^{\frac{1}{2}} \\
\Rightarrow \left(\psi_{1s}^{\frac{1}{2}}\right)^{(1z)} &\approx \frac{n\omega_0}{2}\cos(\omega_0 z)\psi_{1s}^{\frac{1}{2}}
\end{aligned}
\tag{22}
$$

3 Simulation Results and Discussions

3.1 Quantization phenomenon

To show how the number of periods N affects the spectrum of the periodic Gaussian basis function $\psi_1(r)$, we first look at simulation results where the spectrum are made from single (N=1) and multiple (N=10) Gaussian beams as in Fig. 6. The results are for $n = 10$, $\lambda = 1$ and $0 \leq r \leq \frac{N}{2}$. We used Matlab Fourier transform function for simulation results. It is clear that the magnitude of single Gaussian Fourier transform $||\Psi_1(\nu)||$ in space domain gives another continuous Gaussian in spatial frequency domain. We know that a FT of a single Gaussian is another Gaussian as in Eq. (10) and Fig. 6. This equation shows the duality of Gaussian parameters between spatial and frequency domains: The Gaussian width in spatial domain is inversely proportional to those in frequency domain ($\alpha_1 = \pi^2/\alpha$). However, multiple Gaussian beams produce a discrete Gaussian in frequency domain. This means that increasing N causes a natural quantization phenomenon in frequency domain, especially when N ≥ 2 as in Eq. (12). This equation shows that the distance between peaks such as spatial frequency resolution is constant and multiple of $\frac{1}{\mu}$=$\frac{4}{\lambda}$.

Now let's observe and interpret the influence of the n parameter in the frequency domain and its link with the quantization phenomenon. The simulation results in Fig. 7 show $||\Psi_1(\nu)||$ for varying n from 1 to 8. The results have been obtained for $N = 10$, $\lambda = 1$ and $0 \leq r \leq 5$. The periodic Gaussian spectra are fully discrete with Gaussian shape. The number of peaks increases with increasing n, and is equal to $n + 1$ as shown in Eq. (13) and (14). However, this parameter does not affect the spectrum behavior and the spatial frequency resolution. Furthermore, the n parameter adjusts the Gaussian bandwidth in the frequency domain, and the maximal frequency is $|nf_0|$=$|\frac{n}{\lambda}|$ as shown in Eq. 13. This can explain the increasing Gaussian width in the frequency domain for increasing n. As a result, the quantization phenomenon occurs only during the analysis of periodic Gaussians in the frequency domain. A single continuous Gaussian in the spatial domain induces another continuous Gaussian in the Fourier domain. This means that if we consider a periodic system in the spatial domain spaced by λ and characterized by the $\psi_3(r)$ function in 3D space, then we will obtain a discrete spectrum in the Fourier domain. However, if we consider a single system, we will obtain a single continuous spectrum in the frequency domain.

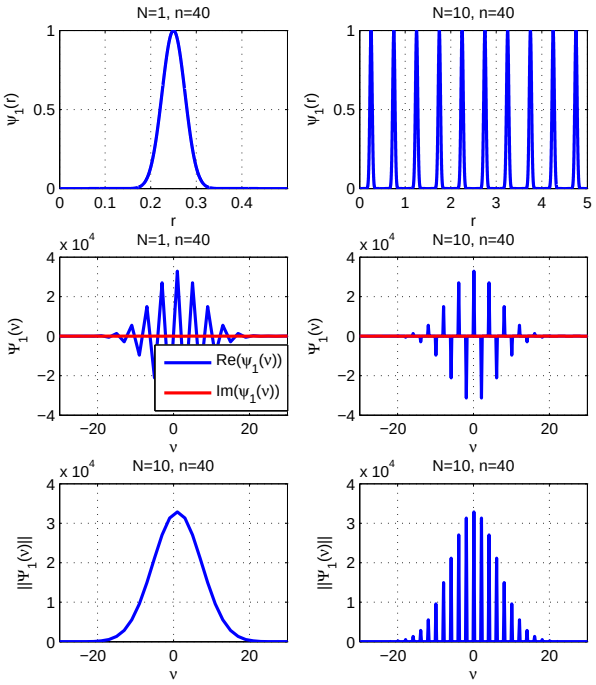

Figure 6: Periodic Gaussian basis function $\psi_1(r)$ and its Fourier transform $\Psi_1(\nu)$ for N=1 and N=10. n is set to 40, $\lambda = 1$, $0 \leq r \leq N\frac{\lambda}{2}$.

Furthermore, as demonstrated in Eq. 16, the binomial coefficients $\binom{n}{i}$ control the magnitude of Periodic Gaussian peaks in the Fourier domain. These coefficients define the Pascal's triangle addresses. The nth row and ith value in Pascal's triangle are indicated by them. They predicted the amplitudes of split NMR peaks using Neutron Magnetic Resonance (NMR) spectroscopy [16, 17]. Moreover, the protons number n in NMR spectroscopy produced $n + 1$ peaks, which are known as the $n + 1$ rule and n lets spin multiplicity. As seen in the images 7 and 8, we can clearly discern a correlation between Periodic Gaussian Fourier analysis and ^{1}H NMR Spectroscopy from these. By analogy, we propose that the Fourier transform of the Periodic Gaussian system structure and the split pattern of NMR spectroscopy are correlated.

3.2 Periodic Gaussian Orbitals

We consider n_n: Principal Quantum Number (QN), l_l: Azimuth QN and m_m: Magnetic QN. The Table. 2 and Figures. 9 to 22 summarize analytical and simulation results. This table shows

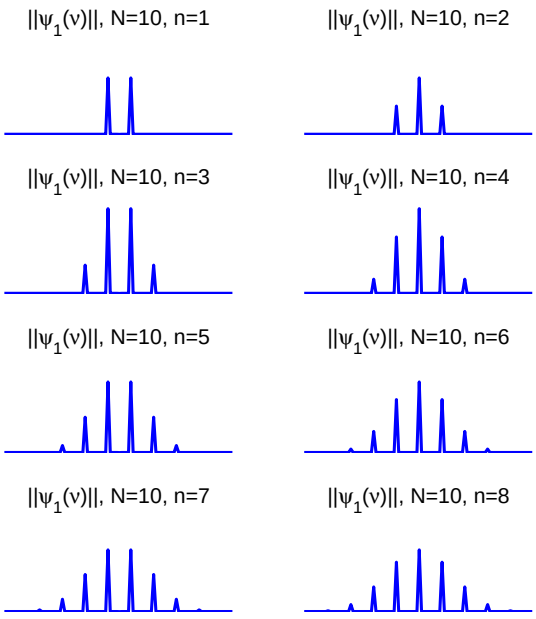

Figure 7: Fourier transform modulus $||\Psi_1(\nu)||$ of Periodic Gaussian basis function versus n parameter. N is set to 10, $\lambda = 1$, $0 \leq r \leq 5$.

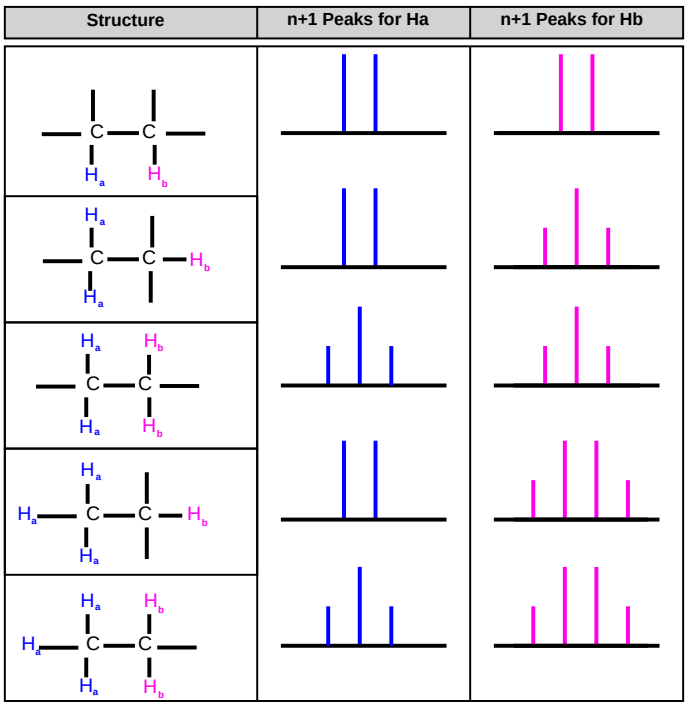

Figure 8: Some examples of splitting patterns, n protons induced $n+1$ peaks known as $n+1$ rule in ^{1}H NMR Spectroscopy.

explicit expanded STO orbitals including 3d-type orbital in the form of canonical Periodic Gaussian-Type Orbitals STO-1PG. The analytical results indicate that entire wavefunctions can be developed exclusively by employing s-type functions in form of canonical STO-1PG. By applying partial primary and secondary derivative like Gradient and Laplacian operators, we can produce orbitals knowing only (1s) wavefunction. As stated in the previous section, the (1s) wavefunction ψ_{1s} like ψ_3 have a spherical form in the 3D space as shows in the Fig. 9 and Table. 2.

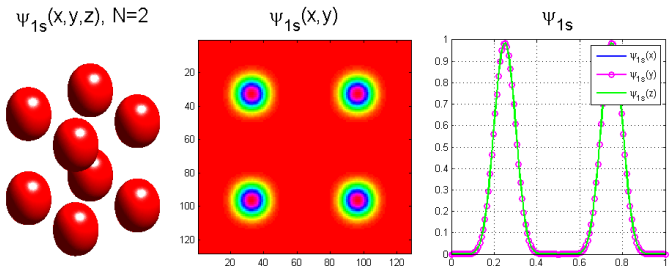

Figure 9: Normalized Periodic $(1s)$ orbital $\psi_{1s}(r)$, N=2, n=10, λ=1, $128\times128\times128$ mesh points.

The (2s) orbital is formed by a linear combination of $\psi_{1s}^{\frac{1}{2}}$ and its first partial derivative, as shown in Fig. 10. The function $\psi_{1s}^{\frac{1}{2}}$ is related to ψ_{1s} by taking the square root of both the Gaussian amplitude and width: $\psi_{1s}^{\frac{1}{2}} \approx A_{1s}^{\frac{1}{2}} \sin^{\frac{n}{2}}(\omega_0 r)$. Similarly, the cube root of ψ_{1s} gives $\psi_{1s}^{\frac{1}{3}}$, and so on. The table shows that only the principal quantum number n_n affects the Gaussian width in the STO-1PG expansion, as $\psi_{1s}^{\frac{1}{nn}} \approx A_{1s}^{\frac{1}{nn}} \sin^{\frac{n}{nn}}(\omega_0 r)$. We can infer from this that the parameter n_n controls the spatial diffusion of Gaussian cells, as illustrated in Fig. 11 [20, 21, 22].

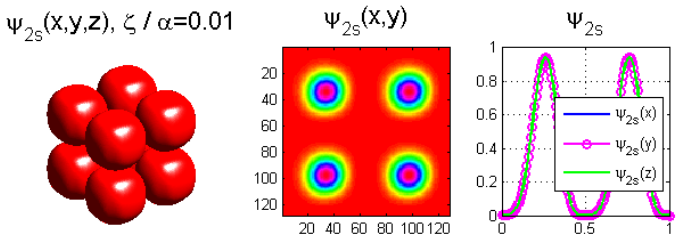

Figure 10: Normalized Periodic $(2s)$ orbital $\psi_{2s}(r)$, N=2, n=10, λ=1, $\frac{\zeta}{\alpha} = 10^{-2}$, $128\times128\times128$ mesh points.

The periodic 2p-type orbitals may be expanded by the directional gradient of $\psi_{1s}^{\frac{1}{2}}$ over (x), (y) or (z) direction as shown in the table. The equation Eq. 21 introduces an explicit approximation of the periodic Gaussian directional gradient. This formula indicates a decrease of the spatial Gaussian width $\psi_{1s}^{\frac{1}{2}}$ compared to ψ_{1s} and also a modulation by $\cos(2\pi f_0 x)$. This induces a symmetric Gaussian spectrum in the spatial frequency domain over $\pm f_0 = \pm\frac{1}{\lambda}$.

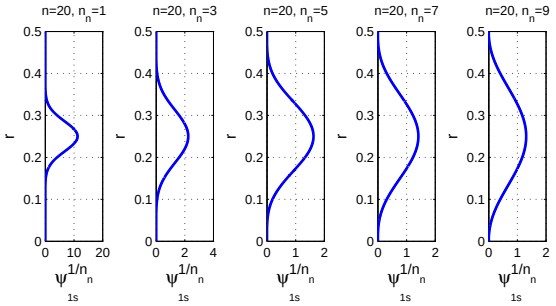

Figure 11: Periodic Gaussian basis function diffusion $\psi_{1s}^{\frac{1}{nn}}(r)$ for N=1, n=20, λ=1, n_n={1,3,5,7,9} (from left to right).

Examples of spatial periodic 2p-type orbitals are illustrated in Figures. 12 and 13 for N=1 and N=2, respectively.

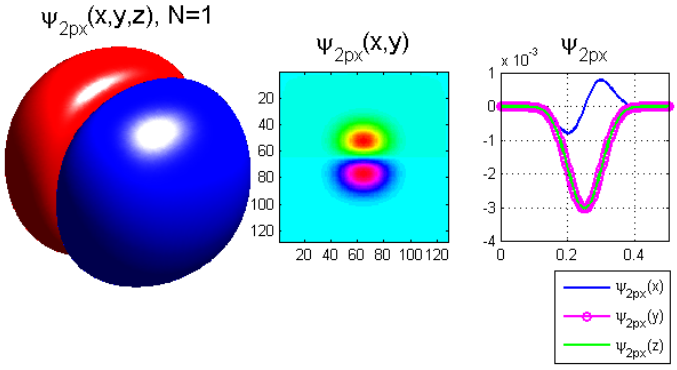

Figure 12: Normalized Periodic ($2px$) orbital $\psi_{2px}(r)$, N=1, n=10, λ=1, 128×128×128 mesh points.

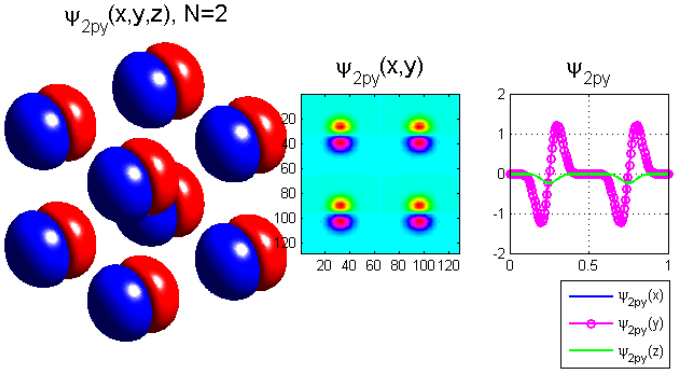

Figure 13: Normalized Periodic ($2py$) orbital $\psi_{2py}(r)$, N=2, n=10, λ=1, 128×128×128 mesh points.

The number of Gaussian cells required to approximate Slater basis function of periodic system in comparison between GTO's expansion and Periodic GTO's in 3D space (m=3) is shown in the Table. 1. The number of the Gaussian cells to approximate a single

Table 1: Comparison of number of Gaussian basis function required to approximate STO-kG and STO-kPG orbitals in Cartesian 3D space versus N, where k being a positive integer.

	Periods Number N					
	1	2	3	4	5	$\forall N$
STO-1G	1	8	27	64	125	$1 \times N^3$
STO-1PG	1	1	1	1	1	1
STO-2G	2	16	54	128	250	$2 \times N^3$
STO-2PG	2	2	2	2	2	2
STO-3G	3	24	81	192	375	$3 \times N^3$
STO-3PG	3	3	3	3	3	3
STO-30G	30	240	810	1920	3750	$30 \times N^3$
STO-30PG	30	30	30	30	30	30
STO-kG	k×1^3	k×2^3	k×3^3	k×4^3	k×5^3	k×N^3
STO-kPG	k	k	k	k	k	k
Cost Gain	**1**	**8**	**27**	**64**	**125**	$\mathbf{N^3}$

Slater-type basis function is given by the positive integer (k). It is clear in the table that the number Gaussian cells growth as the cube of the number of periods (N) and linear proportional to (k) parameter, it raised from 1 (STO-1G, N=1) to 125 (STO-1G, N=5). However, a single periodic Gaussian is sufficient in case of STO-1PG, $\forall N$. As result, the gain between STO-kG and STO-kPG in terms of single Gaussian cell reach N^3 in 3D space. As a conclusion, by applying Periodic Gaussian, the computation cost of periodic system may be dramatically reduced by N^3 compared to the basic Gaussian cell [23, 24, 25, 26]. This is due to natural periodicity of sinusoidal function.

The table shows how many Gaussian cells are needed to approximate a Slater basis function of a periodic system, using either GTO's expansion or Periodic GTO's in 3D space (m=3). The number of Gaussian cells for one Slater-type basis function is determined by the positive integer (k). The table reveals that the number of Gaussian cells increases with the cube of the number of periods (N) and is linearly proportional to (k). It goes from 1 (STO-1G, N=1) to 125 (STO-1G, N=5). However, only one periodic Gaussian is enough for STO-1PG, regardless of N. Therefore, the advantage of using STO-kG over STO-kPG in terms of single Gaussian cell is N^3 in 3D space. In conclusion, periodic Gaussians can reduce the computational cost of periodic systems by N^3 compared to basic Gaussian cells [23, 24, 25, 26], because of the natural periodicity of sinusoidal functions.

However, in GTO expansions, it is well known that the number of Gaussian basis functions required to achieve better approximations of Slater-type orbitals may be important. In this study we limited to first approximation of STO's in terms of GTO's. This may represent a primary approximation of electron behavior over the nucleus. The higher number of Gaussian basis functions to approximate Periodic Gaussian function have not yet been investigated. We believe that the mathematical complexity of molecular computation will be reduced by using Periodic Gaussian

basis function. These orbitals will be describing electrons behavior such as a linear combination of sine a cosine functions. In addition, we postulate existence of correlation between Periodic Gaussian Fourier transform and NMR molecular spectrum. The inspection of these hypotheses is now in progress.

One challenge of using GTO expansions is that they need many Gaussian basis functions to approximate Slater-type orbitals more accurately. In this study, we used the first approximation of STO's by GTO's. This is a basic way of modeling the electron behavior near the nucleus. We have not explored the use of more Gaussian basis functions to approximate Periodic Gaussian functions. We think that Periodic Gaussian basis functions can simplify the mathematical calculations of molecular systems. We used orbitals to model how electrons behave as a linear combination of sine and cosine functions. We also proposed a connection between the Periodic Gaussian Fourier transform and the NMR molecular spectrum. The inspection of these hypotheses is now in progress.

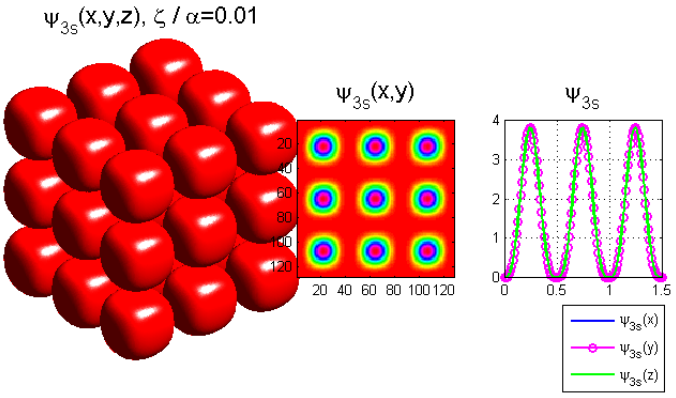

Figure 14: Normalized Periodic $(3s)$ orbital $\psi_{3s}(r)$, N=3, n=10, λ=1, 128×128×128 mesh points.

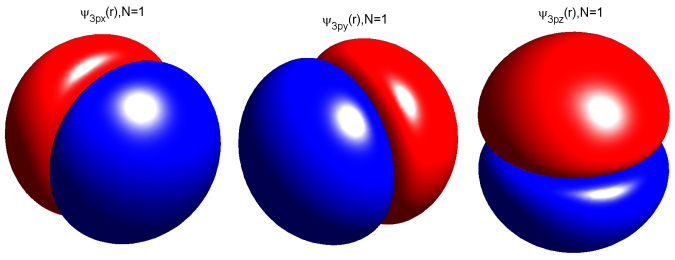

Figure 15: Normalized Periodic $(3px)$, $(3py)$ and $(3pz)$ orbitals, N=1, n=10, λ=1, 128×128×128 mesh points.

4 Appendix

Let $\psi_{3s}(r)$, $\psi_{3px}(r)$, $\psi_{3py}(r)$,..., $\psi_{3d2}(r)$ denote the rest of nine wavefunctions including 3d-type orbitals. The approximate canon-

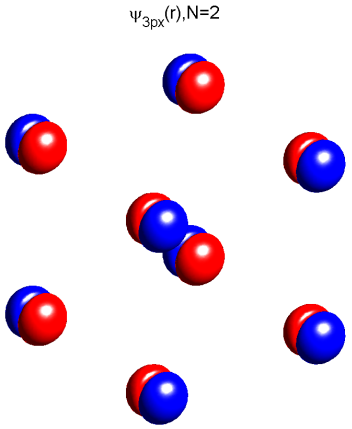

Figure 16: Normalized Periodic $(3px)$ orbital $\psi_{3px}(r)$, N=2, n=10, λ=1, 128×128×128 mesh points.

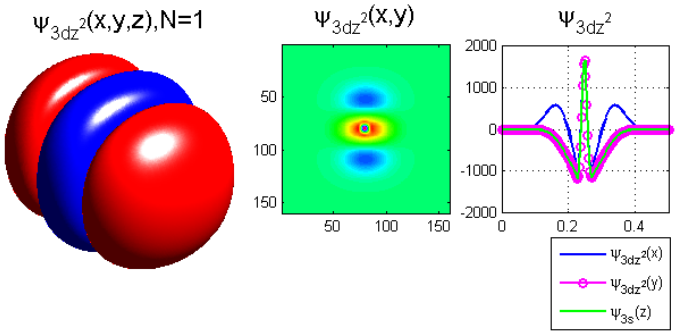

Figure 17: Normalized Periodic $(3d_{z^2})$ orbital, N=1, n=3x10, λ=1, 128×128×128 mesh points.

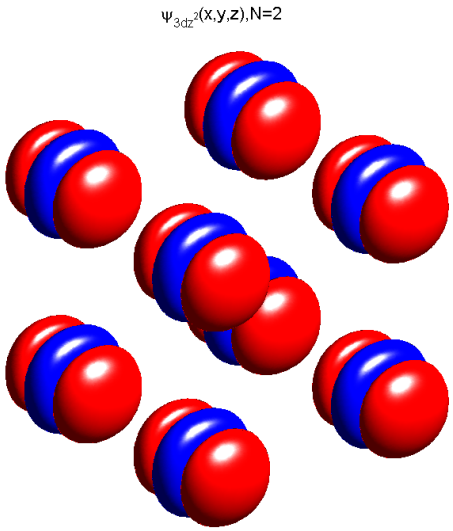

Figure 18: Normalized Periodic $(3d_{z^2})$ orbital, N=2, n=3x10, λ=1, 128×128×128 mesh points.

Table 2: Explicit Primary Slater-Type Orbitals STO's and corresponding canonical Periodic Gaussian-Type Orbitals STO-1PG involving 1s Wavefunction $\psi_{1s}(r)$.

N	Orbital	(n_n, l_l, m_m)	Explicit STO's Orbitals	Canonical STO-1PG Orbitals (Eq.), Fig.
2	**1s**	(1, 0, 0)	$\psi_{1s}(r) = A_{1s}\exp\Big(-\xi r\Big),\ A_{1s} = \sqrt{\frac{\xi^3}{\pi}}$	$\psi_{1s}(r) \approx B'_{1s}\psi_3(r)$ (19), 9
2	**2s**	(2, 0, 0)	$\psi_{2s}(r) = \frac{A_{2s}}{\sqrt{A_{1s}}}\Big(2-\zeta r\Big)\psi_{1s}^{\frac{1}{2}},\ A_{2s} = \sqrt{\frac{\xi^3}{32\pi}}$	$\psi_{2s}(r) \approx A'_{2s}\Big(2\psi_{1s}^{\frac{1}{2}} + \frac{\zeta}{\alpha}\Big(\psi_{1s}^{\frac{1}{2}}\Big)^{(1)}\Big)$ (20), 10
1	**2px**	(2, 1, -1)	$\psi_{2px}(r) = \frac{\zeta A_{2px}}{\sqrt{A_{1s}}}x\psi_{1s}^{\frac{1}{2}},\ A_{2px} = A_{2s}$	$\psi_{2px}(r) \approx -A'_{2px}\frac{\zeta}{\alpha}\Big(\psi_{1s}^{\frac{1}{2}}\Big)^{(1x)}$ (21), 12
2	**2py**	(2, 1, 1)	$\psi_{2py}(r) = \frac{\zeta A_{2py}}{\sqrt{A_{1s}}}y\psi_{1s}^{\frac{1}{2}},\ A_{2py} = A_{2s}$	$\psi_{2py}(r) \approx -A'_{2py}\frac{\zeta}{\alpha}\Big(\psi_{1s}^{\frac{1}{2}}\Big)^{(1y)}$ (21), 13
	2pz	(2, 1, 0)	$\psi_{2pz}(r) = \frac{\zeta A_{2pz}}{\sqrt{A_{1s}}}z\psi_{1s}^{\frac{1}{2}},\ A_{2pz} = A_{2s}$	$\psi_{2pz}(r) \approx -A'_{2pz}\frac{\zeta}{\alpha}\Big(\psi_{1s}^{\frac{1}{2}}\Big)^{(1z)}$ (21)
3	**3s**	(3, 0, 0)	$\psi_{3s}(r) = A'_{3s}\Big(27 - 18\zeta r + 2(\zeta r)^2\Big)\psi_{1s}^{\frac{1}{3}}$ $A'_{3s} = \frac{1}{81A_{1s}^{\frac{1}{3}}}\sqrt{\frac{\zeta^3}{3\pi}}$	$\psi_{3s}(r) \approx A^0_{3s}\Big(\psi_{1s}^{\frac{1}{3}}\Big) + A^1_{3s}\Big(\psi_{1s}^{\frac{1}{3}}\Big)^{(1)}$ $+A^2_{3s}\Big(\psi_{1s}^{\frac{1}{3}}\Big)^{(2)}$ (23), 14
1	**3pz**	(3, 1, 0)	$\psi_{2pz}(r) = A'_{3pz}z\Big(6-\zeta r\Big)\psi_{1s}^{\frac{1}{3}}$	$\psi_{3pz}(r) \approx -A''_{3pz}\cos(\omega_0 z)\Big(6\psi_{1s}^{\frac{1}{3}} + \frac{3\zeta}{2\alpha}\Big(\psi_{1s}^{\frac{1}{3}}\Big)^{(1)}\Big)$ (24), 15
1	**3py**	(3, 1, 1)	$\psi_{2py}(r) = A'_{3py}y\Big(6-\zeta r\Big)\psi_{1s}^{\frac{1}{3}}$	$\psi_{3py}(r) \approx -A''_{3py}\cos(\omega_0 y)\Big(6\psi_{1s}^{\frac{1}{3}} + \frac{3\zeta}{2\alpha}\Big(\psi_{1s}^{\frac{1}{3}}\Big)^{(1)}\Big)$ (24), 15
1,2	**3px**	(3, 1, -1)	$\psi_{2px}(r) = A'_{3px}x\Big(6-\zeta r\Big)\psi_{1s}^{\frac{1}{3}}$	$\psi_{3px}(r) \approx -A''_{3px}\cos(\omega_0 x)\Big(6\psi_{1s}^{\frac{1}{3}} + \frac{3\zeta}{2\alpha}\Big(\psi_{1s}^{\frac{1}{3}}\Big)^{(1)}\Big)$ (24), 16, 15
1,2	**3d**z^2	(3, 2, 0)	$\psi_{3dz2}(r) = A'_{3dz2}\Big(3z^2 - r^2\Big)\psi_{1s}^{\frac{1}{3}}$	$\psi_{3dz^2}(r) \approx A''_{3dz2}\Big(3\Big(\psi_{1s}^{\frac{1}{3}}\Big)^{(2z)} - \Big(\psi_{1s}^{\frac{1}{3}}\Big)^{(2)} + 4\alpha'\psi_{1s}^{\frac{1}{3}}\Big)$ (25), 17, 18
5	**3dxz**	(3, 2, -1)	$\psi_{3dxz}(r) = A'_{3dxz}xz\psi_{1s}^{\frac{1}{3}}$	$\psi_{3dxz}(r) \approx \frac{A'_{3dxz}}{(2\alpha')^2}\Big(\psi_{1s}^{\frac{1}{3}}\Big)^{(1x)}\Big(\psi_{1s}^{\frac{1}{3}}\Big)^{(1z)}\cdot \psi_{1s}^{-\frac{1}{3}}$ (25), 21,19,20
1	**3dyz**	(3, 2, 1)	$\psi_{3dyz}(r) = A'_{3dyz}yz\psi_{1s}^{\frac{1}{3}}$	$\psi_{3dyz}(r) \approx \frac{A'_{3dyz}}{(2\alpha')^2}\Big(\psi_{1s}^{\frac{1}{3}}\Big)^{(1y)}\Big(\psi_{1s}^{\frac{1}{3}}\Big)^{(1z)}\cdot \psi_{1s}^{-\frac{1}{3}}$ (25), 19
1	**3dxy**	(3, 2, -2)	$\psi_{3dxy}(r) = A'_{3dxy}xy\psi_{1s}^{\frac{1}{3}}$	$\psi_{3dxy}(r) \approx \frac{A'_{3dxy}}{(2\alpha')^2}\Big(\psi_{1s}^{\frac{1}{3}}\Big)^{(1x)}\Big(\psi_{1s}^{\frac{1}{3}}\Big)^{(1y)}\cdot \psi_{1s}^{\frac{1}{3}}$ (25), 19
2	**3d**$_{x^2-y^2}$	(3, 2, 2)	$\psi_{3d2}(r) = A'_{3d2}\Big(x^2 - y^2\Big)\psi_{1s}^{\frac{1}{3}},$ $A_{3d2} = \frac{1}{81}\sqrt{\frac{2\zeta^3}{\pi}}$	$\psi_{3d2}(r) \approx \Big(\frac{n'\omega_0}{2\alpha'}\Big)^2 A'_{3d2}\cdot\psi_{1s}^{-\frac{1}{3}}\cdot \Big[\Big(\psi_{1s}^{\frac{1}{3}\,(1x)}\Big)^2 - \Big(\psi_{1s}^{\frac{1}{3}\,(1y)}\Big)^2\Big]$ (27)

N: Periods number, n_n: Principal Quantum Number (QN), l_l: Azimuth QN, m_m: Magnetic QN
$r = r\{x, y, z\} = \sqrt{x^2 + y^+ z^2}$: Electron distance from the nucleus in Cartesian coordinates
$A_{1s}, A_{1s}, ..., A_{3d2}$: Normalization constants of Slater basis functions
$B_{1s}, B'_{1s}, ..., B'_{3d2}$: Normalization constants of Periodic Gaussian basis functions

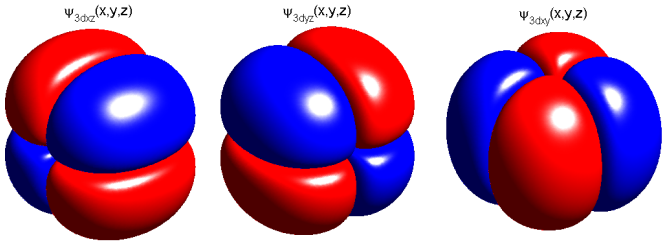

Figure 19: Normalized Periodic $(3d_{xz})$, $(3d_{yz})$ and $(3d_{xy})$ orbitals, N=1, n=3x10, λ=1, 128×128×128 mesh points.

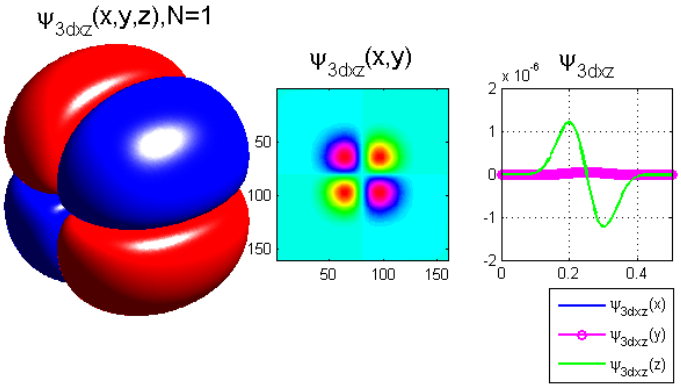

Figure 20: Normalized Periodic $(3d_{xz})$ orbital, N=1, n=3x10, λ=1, 128×128×128 mesh points.

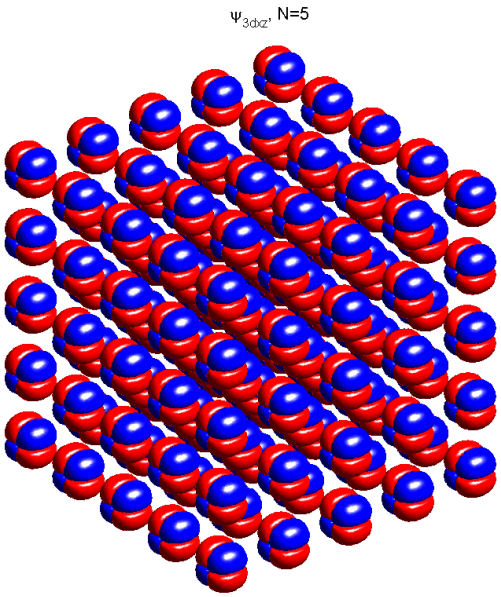

Figure 21: Normalized Periodic $(3d_{xz})$ orbital, N=5, n=3x10, λ=1, 128×128×128 mesh points.

ical formulas are given in equations (23) to (27).

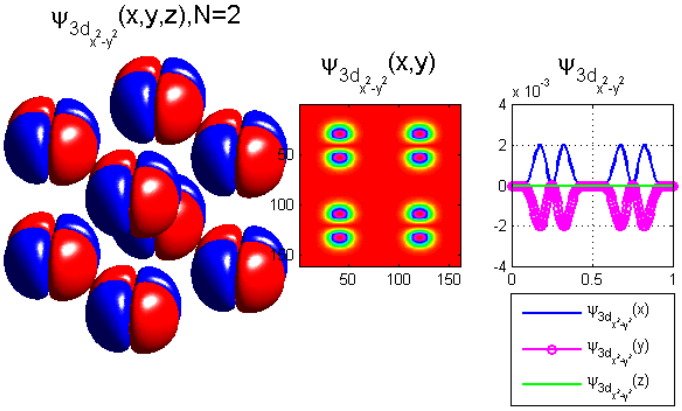

Figure 22: Normalized Periodic $(3d_{x^2-y^2})$ orbital, N=2, n=3x10, λ=1, 128×128×128 mesh points.

$$
\begin{aligned}
\psi_{3s}(r) &= A_{3s}\left(27-18\zeta r+2(\zeta r)^2\right)\exp\left(-\frac{\zeta}{3}r\right),\\
where\ A_{3s} &= \frac{1}{81}\sqrt{\frac{\zeta^3}{3\pi}}\\
let\ \psi_{1s}^{\frac{1}{3}} &= A_{1s}^{\frac{1}{3}}\exp\left(-\frac{\zeta}{3}r\right)\approx B_{1s}^{\frac{1}{3}}\exp\left(-\frac{\alpha}{3}r^2\right)\\
&\Rightarrow \exp\left(-\frac{\zeta}{3}r\right)=\left(\frac{\psi_{1s}}{A_{1s}}\right)^{\frac{1}{3}}\\
then\ \psi_{3s}(r) &= A_{3s}\left(27-18\zeta r+2(\zeta r)^2\right)\left(\frac{\psi_{1s}}{A_{1s}}\right)^{\frac{1}{3}}\\
&= \underbrace{\frac{A_{3s}}{A_{1s}^{\frac{1}{3}}}}_{A'_{3s}}\left(27-18\zeta r+2(\zeta r)^2\right)\psi_{1s}^{\frac{1}{3}}\\
let\ \left(\psi_{1s}^{\frac{1}{3}}\right)^{(1)} &= \frac{\partial}{\partial r}\left(\psi_{1s}^{\frac{1}{3}}\right)=-\frac{2}{3}\alpha r\left(\psi_{1s}^{\frac{1}{3}}\right)\\
&\Rightarrow r\left(\psi_{1s}^{\frac{1}{3}}\right)=-\frac{3}{2\alpha}\left(\psi_{1s}^{\frac{1}{3}}\right)^{(1)}\\
and\ \left(\psi_{1s}^{\frac{1}{3}}\right)^{(2)} &= \frac{\partial^2}{\partial r^2}\left(\psi_{1s}^{\frac{1}{3}}\right)\\
&= -\frac{2}{3}\alpha\left(\psi_{1s}^{\frac{1}{3}}\right)+\left(\frac{2\alpha}{3}\right)^2 r^2\left(\psi_{1s}^{\frac{1}{3}}\right)\\
\Rightarrow r^2\left(\psi_{1s}^{\frac{1}{3}}\right) &= \left(\frac{3}{2\alpha}\right)^2\left(\left(\psi_{1s}^{\frac{1}{3}}\right)^{(2)}+\frac{2\alpha}{3}\left(\psi_{1s}^{\frac{1}{3}}\right)\right)\\
then\ \psi_{3s}(r) &\approx A'_{3s}\left(27\psi_{1s}^{\frac{1}{3}}+27\frac{\zeta}{\alpha}\left(\psi_{1s}^{\frac{1}{3}}\right)^{(1)}+\right.\\
&\quad \left.2\left(\frac{3\zeta}{2\alpha}\right)^2\left(\left(\psi_{1s}^{\frac{1}{3}}\right)^{(2)}+\frac{2\alpha}{3}\left(\psi_{1s}^{\frac{1}{3}}\right)\right)\right)\\
&\approx A_{3s}^0\left(\psi_{1s}^{\frac{1}{3}}\right)+A_{3s}^1\left(\psi_{1s}^{\frac{1}{3}}\right)^{(1)}+A_{3s}^2\left(\psi_{1s}^{\frac{1}{3}}\right)^{(2)},\\
where\ A_{3s}^0 &= A'_{3s}\left(27+\frac{3\zeta^2}{\alpha}\right),\ A_{3s}^1=27A'_{3s}\frac{\zeta}{\alpha},\\
A_{3s}^2 &= 2A'_{3s}\left(\frac{3\zeta}{2\alpha}\right)^2
\end{aligned}
\tag{23}
$$

$$
\begin{aligned}
\psi_{3pz}(r) &= A_{3pz} z\Big(6-\zeta r\Big)\exp\Big(-\frac{\zeta}{3}r\Big),\\
A_{3pz} &= \frac{1}{81}\sqrt{\frac{2\zeta^5}{\pi}}\\
&= \frac{A_{3pz}}{A_{1s}^{\frac{1}{3}}} z\Big(6-\zeta r\Big)\psi_{1s}^{\frac{1}{3}} = A'_{3pz} z\Big(6-\zeta r\Big)\psi_{1s}^{\frac{1}{3}}\\
let\ \Big(\psi_{1s}^{\frac{1}{3}}\Big)^{(1)} &= -\frac{2}{3}\alpha r\psi_{1s}^{\frac{1}{3}} \Rightarrow r\psi_{1s}^{\frac{1}{3}} \approx -\frac{3}{2\alpha}\Big(\psi_{1s}^{\frac{1}{3}}\Big)^{(1)}\\
and\ \Big(\psi_{1s}^{\frac{1}{3}}\Big)^{(1z)} &\approx A_{1s}^{\frac{1}{3}}\frac{n}{3}\omega_0\cos(\omega_0 z)\sin^{\frac{n}{3}-1}(\omega_0 z)\\
&\quad\cdot\Big(\sin(\omega_0 x)\sin(\omega_0 y)\Big)^{\frac{n}{3}}\\
\frac{n}{3} >> 1 \Rightarrow \Big(\psi_{1s}^{\frac{1}{3}}\Big)^{(1z)} &\approx \frac{n\omega_0}{3}\cos(\omega_0 z)\psi_{1s}^{\frac{1}{3}} \approx -\frac{2\alpha}{3} z\psi_{1s}^{\frac{1}{3}}\\
&\Rightarrow z \approx -\frac{n\omega_0}{2\alpha}\cos(\omega_0 z)\\
then:\ \psi_{3pz}(r) &\approx -\underbrace{A'_{3pz}\frac{n\omega_0}{2\alpha}}_{A''_{3pz}}\cos(\omega_0 z)\Big(6\psi_{1s}^{\frac{1}{3}} + \frac{3\zeta}{2\alpha}\Big(\psi_{1s}^{\frac{1}{3}}\Big)^{(1)}\Big)\\
\psi_{3py}(r) &\approx -A''_{3py}\cos(\omega_0 y)\Big(6\psi_{1s}^{\frac{1}{3}} + \frac{3\zeta}{2\alpha}\Big(\psi_{1s}^{\frac{1}{3}}\Big)^{(1)}\Big)\\
\psi_{3px}(r) &\approx -A''_{3px}\cos(\omega_0 x)\Big(6\psi_{1s}^{\frac{1}{3}} + \frac{3\zeta}{2\alpha}\Big(\psi_{1s}^{\frac{1}{3}}\Big)^{(1)}\Big)
\end{aligned}
\tag{24}
$$

$$
\begin{aligned}
\psi_{3dz2}(r) &= A_{3dz2}\Big(3z^2-r^2\Big)\exp\Big(-\frac{\zeta}{3}r\Big)\\
&= \frac{A_{3dz2}}{A_{1s}^{\frac{1}{3}}}\Big(3z^2-r^2\Big)\psi_{1s}^{\frac{1}{3}} = A'_{3dz2}\Big(3z^2-r^2\Big)\psi_{1s}^{\frac{1}{3}}\\
&\approx \frac{A'_{3dz2}}{(2\alpha')^2}\Big(3\Big(\psi_{1s}^{\frac{1}{3}}\Big)^{(2z)} - \Big(\psi_{1s}^{\frac{1}{3}}\Big)^{(2)} + 4\alpha'\psi_{1s}^{\frac{1}{3}}\Big),\\
where\ \alpha' &= \frac{\alpha}{3},\ A_{3dz2} = \frac{1}{81}\sqrt{\frac{\zeta^3}{6\pi}}
\end{aligned}
\tag{25}
$$

$$
\begin{aligned}
\psi_{3dxz}(r) &= A_{3dxz} xz\exp\Big(-\frac{\zeta}{3}r\Big),\ A_{3dxz} = \frac{1}{81}\sqrt{\frac{2\zeta^3}{\pi}}\\
&= \frac{A_{3dxz}}{A_{1s}^{\frac{1}{3}}} xz\psi_{1s}^{\frac{1}{3}} = A'_{3dxz} xz\psi_{1s}^{\frac{1}{3}}\\
xz\psi_{1s}^{\frac{1}{3}} &\approx \frac{1}{(2\alpha')^2}\Big(\psi_{1s}^{\frac{1}{3}}\Big)^{(1x)}\Big(\psi_{1s}^{\frac{1}{3}}\Big)^{(1z)}\cdot\psi_{1s}^{-\frac{1}{3}}\\
&\approx \Big(\frac{n'\omega_0}{2\alpha'}\Big)\cos(\omega_0 x)\cos(\omega_0 z)\Big(\sin^{(n'-1)}(\omega_0 x)\cdot\\
&\quad\sin^{n'}(\omega_0 y)\sin^{(n'-1)}(\omega_0 z)\Big),\ \forall\ \psi_{1s}^{\frac{1}{3}}\\
&\approx \frac{\psi_{3dxz}(r)}{A'_{3dxz}},\ \alpha' = \frac{\alpha}{3},\ n' = \frac{n}{3}\\
yz\psi_{1s}^{\frac{1}{3}} &\approx \frac{1}{(2\alpha')^2}\Big(\psi_{1s}^{\frac{1}{3}}\Big)^{(1y)}\Big(\psi_{1s}^{\frac{1}{3}}\Big)^{(1y)}\cdot\psi_{1s}^{-\frac{1}{3}}\\
xy\psi_{1s}^{\frac{1}{3}} &\approx \frac{1}{(2\alpha')^2}\Big(\psi_{1s}^{\frac{1}{3}}\Big)^{(1x)}\Big(\psi_{1s}^{\frac{1}{3}}\Big)^{(1y)}\cdot\psi_{1s}^{-\frac{1}{3}}
\end{aligned}
\tag{26}
$$

$$
\begin{aligned}
\psi_{3d2}(r) &= A_{3d2}\Big(x^2-y^2\Big)\exp\Big(-\frac{\zeta}{3}r\Big),\ A_{3d2} = \frac{1}{81}\sqrt{\frac{2\zeta^3}{\pi}}\\
&= \frac{A_{3d2}}{A_{1s}^{\frac{1}{3}}}\Big(x^2-y^2\Big)\psi_{1s}^{\frac{1}{3}} = A'_{3d2}\Big(x^2-y^2\Big)\psi_{1s}^{\frac{1}{3}}\\
let\ x^2\psi_{1s}^{\frac{1}{3}} &\approx \frac{1}{(2\alpha')^2}\Big(\psi_{1s}^{\frac{1}{3}}\Big)^{(1x)}\Big(\psi_{1s}^{\frac{1}{3}}\Big)^{(1x)}\cdot\psi_{1s}^{-\frac{1}{3}}\\
&\approx \Big(\frac{n'\omega_0}{2\alpha'}\Big)^2\cos^2(\omega_0 x)\Big(\sin^{(n'-2)}(\omega_0 x)\cdot\\
&\quad\sin^{n'}(\omega_0 y)\sin^{n'}(\omega_0 z)\Big),\ \alpha' = \frac{\alpha}{3},\ n' = \frac{n}{3}\\
and\ y^2\psi_{1s}^{\frac{1}{3}} &\approx \frac{1}{(2\alpha')^2}\Big(\psi_{1s}^{\frac{1}{3}}\Big)^{(1y)}\Big(\psi_{1s}^{\frac{1}{3}}\Big)^{(1y)}\cdot\psi_{1s}^{-\frac{1}{3}}\\
&\approx \Big(\frac{n'\omega_0}{2\alpha'}\Big)^2\cos^2(\omega_0 y)\Big(\sin^{n'}(\omega_0 x)\cdot\\
&\quad\sin^{(n'-2)}(\omega_0 y)\sin^{n'}(\omega_0 z)\Big)\\
then\ \psi_{3d2}(r) &\approx \Big(\frac{n'\omega_0}{2\alpha'}\Big)^2 A'_{3d2}\cdot\psi_{1s}^{-\frac{1}{3}}\Big[\Big(\psi_{1s}^{\frac{1}{3}(1x)}\Big)^2 -\\
&\quad\Big(\psi_{1s}^{\frac{1}{3}(1y)}\Big)^2\Big]
\end{aligned}
\tag{27}
$$

Acknowledgments

The authors would like to thank the reviewers for their criticisms, comments and suggestions.

Data availability

Matlab scripts for figures reproduction are available on request from the corresponding author.

References:

[1] John C. Slater. *Atomic Shielding Constants*. Physical Review, vol.36, page 57, 1930.

[2] Victor Garcia1, David Zorrilla et al. *Software to obtain accurate Gaussian expansions for a wide range of radial functions*. J Mol Model (2017) 23: 165, doi 10.1007/s00894-017-3340-x, 2017.

[3] J. L. WmTTEN. *Gaussian Lobe Function Expansions of Hartree-Fock Solutions for the First-Row Atoms and Ethylene*. The Journal of Chimical Physics, vol.44, 1966.

[4] D.F. Brailsford et al. *Floating s- and p-type Gaussian Orbitals*. Chemial Physics Letters vol.35, number 4, 1975.

[5] Guseinov II, Erturk M. *Use of noninteger nSlater type orbitals in combined Hartree-Fock-Roothaan theory for calculation of isoelectronic series of atoms*. Be to Ne. International Journal of Quantum Chemistry, 109(2):176-184. doi: https://doi.org/10.1002/qua.21760, 20, 2009.

[6] Daniel A. Morales. *On the evaluation of integrals with Coulomb Sturmian radial functions*. J Math Chem (2016) 54:682689, doi 10.1007/s10910-015-0588-1, 2016.

[7] Micha Lesiuk. *Calculation of STOs electron repulsion integrals by ellipsoidal expansion and large-order approximations*. J Math Chem 54:572591, doi 10.1007/s10910-015-0576-5, 2016.

[8] Cory C. Pye and Colin J. Mercer. *On the Least-Squares Fitting of Slater-Type Orbitals with Gaussians: Reproduction of the STONG Fits Using Microsoft Excel and Maple*. The Journal of Chemical Education, dx.doi.org/10.1021/ed300032f — J. Chem. Educ. 2012, 89, 14051410, 2012.

[9] Brianna Stewart et al. *A Systematic Approach for Understanding SlaterGaussian Functions in Computational Chemistry*. dx.doi.org/10.1021/ed300807y, J. Chem. Educ. , 90, 609612, 2013.

[10] TYygve Helgaker and Peter R. Taylor. *Chapter 12: Gaussian Bais Sets and Molecular Integrals*. Department of Chemistry, University of Oslo, Modern Electronic Structure Theory Downloaded, 2013.

[11] Kiyosi O-ohata, Hiroshi Taketa and Sigeru Huzinaga. *Gaussian Expansions of Atomic Orbitals*. Journal of the Physical Society of Japan, No. 21, No. 11, 1966.

[12] James M. LeBeau, Scott D. Findlay et al. *Standardless Atom Counting in Scanning Transmission Electron Microscopy*. doi: 10.1021/nl102025s, Nano Lett, 10, 44054408, 2010.

[13] Ondrej L. Krivanek1, Matthew F. Chisholm et al. *Atom-by-atom structural and chemical analysis by annular dark-field electron microscopy*. Nature Letters, Vol 464, doi:10.1038/nature08879, 2010.

[14] Jiamin Xue, Javier Sanchez-Yamagishi et al. *STM Spectroscopy of ultra-flat graphene on hexagonal boron nitride*. arXiv:1102.2642v1, 2011.

[15] EH. Ait Mansour and S. Barth. *Efficient Approximation of Gaussian Function for Signal and Image Processing Applications*. IEEE Signal Processing Symposium (SPSympo-2019), Sept. 2019.

[16] James Keeler. *Understanding NMR Spectroscopy*. University of Cambridge, Department of Chemistry, 2002.

[17] Erin M. Kolonko, and Kristopher J. Kolonko. *Introducing NMR Spectroscopy Using Guided Inquiry and Partial Structure Templating*. J. Chem. Educ. 2019, 96, 912919, 2019.

[18] Andrew B. Yankovich, Benjamin Berkels et al. *Picometre-precision analysis of scanning transmission electron microscopy images of platinum nanocatalysts*. , Nature communications, doi: 10.1038/ncomms5155, 2014.

[19] Mukherjee et al. *mpfit: a robust method for fitting atomic resolution images with multiple Gaussian peaks*. doi.org/10.1186/s40679-020-0068-y, Adv Struct Chem Imag 6:1, 2020.

[20] R. Nicholas Lanning, Zhihao Xiao et al. *Gaussian Beam-Propagation Theory for Nonlinear Optics Featuring an Exact Treatment of Orbital Angular Momentum Transfer*. arXiv:1702.01095v2 [physics.optics], 2017.

[21] Juan Luis Vazquez. *The mathematical theories of diffusion. Nonlinear and fractional diffusion*. arXiv:1706.08241v1 [math.AP], 2017.

[22] A.D. McDonald, K. Woodruff et al. *Electron Drift and Longitudinal Diffusion in High Pressure Xenon-Helium Gas Mixtures*. JINST, arXiv:1902.05544v4 [physics.ins-det], 2019.

[23] Roman Lazarski, Asbjorn M. Burow et al. *Density Functional Theory for Molecular and Periodic Systems Using Density Fitting and Continuous Fast Multipole Methods*. DOI: 10.1021/acs.jctc.5b00252 J. Chem. Theory Comput. 2015, 11, 30293041, 2015.

[24] Anil Damle, Lin Lin, and Lexing Ying. *Compressed Representation of KohnSham Orbitals via Selected Columns of the Density Matrix*. DOI: 10.1021/ct500985f, J. Chem. Theory Comput. 2015, 11, 14631469, 2014.

[25] Cesare Pisani, Martin Schutz et al. *CRYSCOR: a program for the post-HartreeFock treatment of periodic systems* . Cite this: Phys. Chem. Chem. Phys., 2012, 14, 76157628, 2012.

[26] Lionel A. Truflandie et al. *Linear scaling implementation of exact exchange using localized numerical orbitals and contraction reduction integrals*. arXiv:1112.5989v2 [physics.chem-ph], 2012.